5635

INTERNATIONAL JOURNAL OF ENERGY RESEARCH
Int. J. Energy Res. 2000; **24**:1257–1276

Solid fuel burning in steady, strained, premixed flow fields: the graphite/air/methane system

Fokion N. Egolfopoulos*,†

Department of Aerospace and Mechanical Engineering, University of Southern California, Los Angeles, CA 90089-1453, U.S.A.

SUMMARY

A detailed numerical investigation was conducted on the simultaneous burning of laminar premixed CH_4/air flames and solid graphite in a stagnation flow configuration. The graphite and methane were chosen for this model, given that they are practical fuels and their chemical kinetics are considered as the most reliable ones among solid and hydrocarbon fuels, respectively. The simulation was performed by solving the quasi-one-dimensional equations of mass, momentum, energy, and species. The GRI 2.1 scheme was used for the gas-phase kinetics, while the heterogeneous kinetics were described by a six-step mechanism including stable and radical species. The effects of the graphite surface temperature, the gas-phase equivalence ratio, and the aerodynamic strain rate on the graphite burning rate and NO_x production and destruction mechanisms were assessed. Results indicate that as the graphite temperature increases, its burning rate as well as the NO_x concentration increase. Furthermore, it was found that by increasing the strain rate, the graphite burning rate increases as a result of the augmented supply of the gas-phase reactants towards the surface, while the NO_x concentration decreases as a result of the reduced residence time. The effect of the equivalence ratio on both the graphite burning rate and NO_x concentration was found to be non-monotonic and strongly dependent on the graphite temperature. Comparisons between results obtained for a graphite and a chemically inert surface revealed that the chemical activity of the graphite surface can result to the reduction of NO through reactions of the CH_3, CH_2, CH, and N radicals with NO.

KEY WORDS: solid fuel; methane combustion; heterogeneous combustion; pollutant emission reduction cofiring

1. INTRODUCTION

While recent advances in laser diagnostics and supercomputing have provided remarkable insight into the very details of the gas phase combustion, the processes controlling the burning of solid fuels in gaseous environments are currently less understood. Solid fuel burning is of particular importance because of its relevance to fires, safety, propulsion, and power generation.

* Correspondence to: Fokion N. Egolfopoulos, Department of Aerospace and Mechanical Engineering, University of Southern California, Los Angeles, CA 90089-1453, U.S.A.
† E-mail: egolfopo@rcf.usc.edu

Contract grant/sponsor: NASA; contract grant/number: NAG3-1877.
Contract grant/sponsor: Fred W. O'Green Assistant Professorship in Engineering.

Received 28 September 1999
Accepted 7 January 2000

Among the various processes controlling the burning of a solid fuel, the less known ones are the heterogeneous chemical kinetics that are typically described by one-step, overall reactions.

Among all solid fuels, the kinetics of graphite are the best understood (e.g. Bradley *et al.*, 1984). Previous studies based on global approaches (e.g. Makino and Law, 1986) included the use of two gasification kinetic steps of the graphite, namely these of O_2 and CO_2, as well as one-step gas-phase oxidation of the resulting CO. Recent semi-global approaches (Cho *et al.*, 1992; Lee *et al.*, 1995; Chelliah *et al.*, 1996) were based on the work of Bradley *et al.* (1984), in which a more detailed, multi-step, heterogeneous reaction scheme was introduced. These studies were conducted in spherical (Cho *et al.*, 1992; Lee *et al.*, 1995) and stagnation flow (Chelliah *et al.*, 1996) configurations, and the gas phase was assumed to be a pure-oxidizing one.

In realistic situations, however, the gas phase may be premixed with fuel(s) at various concentrations. Under such conditions, it is reasonable to anticipate that the gas-phase chemical activity will affect the heterogeneous processes and *vice versa* (e.g. Ronney *et al.*, 1994; Honda and Ronney, 1996). A profound example of such conditions, is the simultaneous combustion of natural gas and coal in cofiring applications, in an attempt to take advantage of the chemical energy of both fuels, and possibly reduce the NO_x emissions. Other examples include flame spread over solid surfaces (e.g. Ronney *et al.*, 1994; Honda and Ronney, 1996) and combustion of dusty flows (e.g. Egolfopoulos and Campbell, 1999), in which the gas phase is already premixed before the initiation of the heterogeneous processes.

Under such conditions, complex thermo-chemical interactions can be established between the two phases. Furthermore, since the temperature of the solid phase can well exceed that of the gas phase flame, it is possible that the levels of NO_x will be affected. These processes can be further complicated by the presence of non-uniform, strained flow fields, which can affect on the one hand, the gas-phase response and on the other, the mass and heat transport to and from the solid phase. Detailed systematic studies of this reacting configuration have yet to appear in the literature.

In view of the above considerations, the main objective of this study was to conduct a detailed numerical simulation and provide physical insight into the details of solid fuel burning in premixed atmospheres, under the presence of non-uniform flow fields. In order to be able to efficiently probe the details of the chemical interactions of such a system, fuels with well-known chemistry were used as a model case. For the solid phase, graphite was chosen given that a reasonable multi-step description of its heterogeneous kinetics exists (Bradley *et al.*, 1984). For the gas phase, methane was chosen given that its chemistry is well-characterized. Furthermore, the simultaneous burning of these two important fuels is of practical importance, as mentioned earlier.

2. NUMERICAL APPROACH

Figure 1 depicts the stagnation flow configuration that is pertinent to the present study. Its numerical simulation was conducted along the stagnation streamline by using the well-established Sandia code package (Kee *et al.*, 1983, 1989). The original opposed-jet code (Kee, 1992) was further modified allowing for the inclusion of thermal radiation in the gas phase and for no-slip velocity boundary conditions at the stagnation plane (Egolfopoulos, 1994a, b; Egolfopoulos *et al.*, 1997). Additional modifications were also made in order to account for the appropriate boundary conditions that allow for the description of the chemical coupling between the two phases.

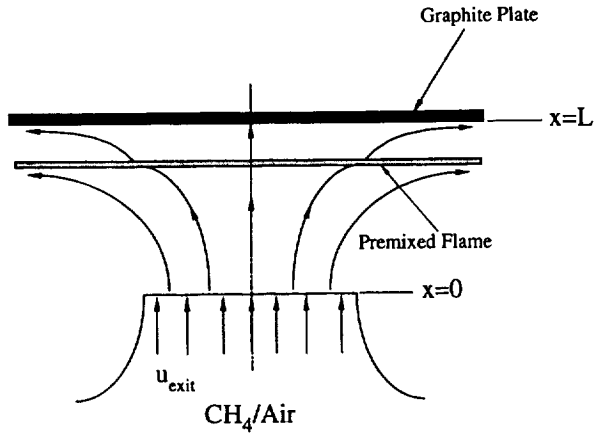

Figure 1. Schematic representation of the stagnation flow configuration.

Similar to previous studies (Cho *et al.*, 1992; Lee *et al.*, 1995; Chelliah *et al.*, 1996), the heterogeneous model of Bradley *et al.* (1984) was used. The scheme includes the following six kinetic steps:

$$\begin{aligned}
C(s) + OH &\rightarrow CO + H, & S1(OH)\\
C(s) + O &\rightarrow CO, & S2(O)\\
C(s) + 4H &\rightarrow CH_4, & S3(H)\\
C(s) + CO_2 &\rightarrow 2CO, & S4(CO_2)\\
C(s) + H_2O &\rightarrow CO + H_2, & S5(H_2O)\\
C(s) + 1/2O_2 &\rightarrow CO, & S6(O_2)
\end{aligned}$$

and the kinetic parameters are those determined in the study of Bradley *et al.* (1984), and identical to the ones used in the previous semi-global studies (Cho *et al.*, 1992; Lee *et al.*, 1995; Chelliah *et al.*, 1996). In the above mechanism, all species are considered to be in the gaseous phase, while C(s) stands for the solid-phase graphite.

It should be emphasized that the above mechanism is only a semi-global one, and that reactions between surface species may be important, but reliable detailed schemes describing them are not currently available (Lee *et al.*, 1995). Furthermore, the graphite porosity has to be considered, when quantitative comparisons with actual experiments are sought (Chelliah *et al.*, 1996).

The S3(H) step was not used in the previous investigations, given that the H would exist in very small concentrations in the gas phase, for example, when trace amounts of H_2O (e.g. 1 per cent) would be added to the gas phase (Lee *et al.*, 1995). In the present study, the postflame region of a methane flame, may contain large concentrations of H and, thus, the S3(H) kinetic step was considered. However, the results that are obtained by using this step must be considered with

caution when quantitative conclusions are sought for the following reasons. First, in the original work of Bradley *et al.* (1984), the temperature range of this step is recommended to be between 303 and 1223 K. Furthermore, Walker *et al.* (1959) are reporting that the surface C(s)–H_2 reaction rate is substantially lower compared to C(s)–H_2O and C–CO_2 reactions at 1073 K, which implies that the contribution of S3(H) to the graphite burning may not be significant. In the present study, it was anticipated that the postflame region in which the graphite is oxidized, may have chemical compositions that are vastly different compared to pure air in which some humidity may be present. For example, while for a fuel-lean case the postflame region may contain large amounts of O_2, CO_2, H_2O, O, and OH and negligible amounts of H, for a fuel-rich flame the postflame region will be dominated by CO, H_2, and H radicals. Such conditions have not been encountered in the previous semi-global studies (Cho *et al.*, 1992; Lee *et al.*, 1995; Chelliah *et al.*, 1996).

In the numerical simulations, the solid-phase temperature was treated as an independent parameter similarly to the studies of Makino and Law (1986) and Chelliah *et al.* (1996). Although one should ideally consider transient effects of the solid phase as recommended by Lee et al. (1995), the parametric study of the solid phase temperature is still valuable, given that it involves the possible values that the graphite is expected to reach during its transient oxidation process, so that the underlying physics can be captured with confidence. Furthermore, the determination of the graphite temperature cannot be uniquely obtained for the geometry studied herein. In the study of Lee *et al.* (1995), the transient response of the graphite temperature was conveniently calculated, given that the geometry of interest was that of a spherical particle.

For the gas-phase kinetics, the GRI 2.1 (Bowman *et al.*, 1995) mechanism was used. The mechanism includes 48 chemical species and 277 reactions of the C_2-hydrocarbon and nitrogen chemistry.

The boundary conditions at the interface were identical to these used by Lee *et al.* (1995). More specifically, the mass fraction of any species at the interface was determined by equating the rate of mass production of the species by all heterogeneous reactions with the total transport (convective + diffusive) of the species at the interface. Furthermore, Stefan flow convection was allowed at the interface as it is induced by the graphite gasification.

Finally, the imposed aerodynamic strain rate, K, was determined as the maximum velocity gradient in the hydrodynamic zone before the heating starts similarly to previous studies (Law, 1988; Egolfopoulos, 1994a, b).

3. RESULTS AND DISCUSSION

The numerical simulations were conducted at atmospheric pressure, and for a separation distance between the nozzle exit and the graphite plate, L, of 10 mm. Three equivalence ratios, ϕ, of the CH_4/air flames were studied, namely 0.7, 1.0, and 1.3. The surface temperature, T_s, was specified to be 1000, 1500, 2000 and 2500 K. The strain rate was varied from very low to near-extinction values for the gas phase; calculations were terminated when convergence was excessively difficult for near-extinction conditions. Independent calculations were also conducted for the same flames impinging on a inert surface, in order to assess the effect of surface chemistry on the NO_x formation.

For all the cases studied herein, the mass burning rate per unit area of the graphite, $R_{c,s}$, by all heterogeneous reactions and the maximum mole fraction in ppm of NO, $X_{NO,max}$ were determined. Representative results of the dependence of $R_{c,s}$ and $X_{NO,max}$ on T_s and K are shown in

Figures 2 and 3, respectively for $\phi = 1.0$. Similar dependence was found for the $\phi = 0.7$ and 1.3 flames with few exceptions, which will be mentioned below.

Effects on the graphite burning rate

The results of Figure 2 indicate that $R_{c,s}$ increases with T_s and K, and a substantial increase is observed between $T_s = 1500$ and 2000 K. For the $\phi = 1.3$ flame and $T_s = 2000$ K a rapid increase of $R_{c,s}$ was found for $K > 500\ s^{-1}$.

The results of Figure 3 indicate that $X_{NO,max}$ increases as T_s increases for a fixed K, and it decreases as K increases for a fixed T_s. Furthermore, it was found that for all ϕs, the $X_{NO,max}$ values are indistinguishable for $T_s = 1000$ and 1500 K, while they are substantially increased at $T_s = 2500$ K. On the other hand, it was found that for the $\phi = 0.7$ flame, the $X_{NO,max}$ values are substantially higher at $T_s = 2000$ K compared to the $T_s = 1500$ K values, with this difference being smaller for the $\phi = 1.0$ flame and near-zero for the $\phi = 1.3$ flame.

The effect of the equivalence ratio, ϕ, on $R_{c,s}$ and $X_{NO,max}$ can be seen in Figures 4–7 for the different surface temperatures.

The results of Figure 4 for $T_s = 1000$ K, indicate that the $\phi = 1.0$ flame results to larger $R_{c,s}$ and $X_{NO,max}$ compared to the $\phi = 0.7$ and 1.3 flames. The $\phi = 0.7$ and 1.3 flames appear to have similar $R_{c,s}$ at $T_s = 1000$ K, but the $X_{NO,max}$ is greater for the $\phi = 1.3$ flame.

The results of Figure 5 for $T_s = 1500$ K, indicate that while the $X_{NO,max}$ behaviour is similar to this for $T_s = 1000$ K, the $\phi = 0.7$ flame results to greater $R_{c,s}$ compared to both the $\phi = 1.0$ and 1.3 flames.

The results of Figure 6 for $T_s = 2000$ K, indicate that while the $R_{c,s}$ for all ϕs become of the same order for most values of K, the $X_{NO,max}$ of the $\phi = 0.7$ flame becomes comparable to the $\phi = 1.0$ flame, increasing thus by an order of magnitude between $T_s = 1500$ and 2000 K. The results of Figure 6 also show a rapid increase of the $R_{c,s}$ for the $\phi = 1.3$ flame and for $K > 500\ s^{-1}$.

The results of Figure 7 for $T_s = 2500$ K, indicate that while the $R_{c,s}$ for all ϕs are very close, the $X_{NO,max}$ values for the $\phi = 0.7$ flame are distinctly greater compared to the $\phi = 1.0$ and 1.3 flames. Furthermore, the $\phi = 1.0$ and 1.3 flames exhibit abrupt reductions of $X_{NO,max}$ values for strain rates greater than 3000 and 200 s^{-1}, respectively.

Figures 6 and 7 also depict $X_{NO,max}$ values that were obtained for the $\phi = 0.7$ and 1.3 flames by replacing the stagnation solid surface with a chemically inert one. Results suggest that the presence of the surface chemistry reduces in general $X_{NO,max}$, with the exception being the $\phi = 0.7$ flame at $T_s = 2000$ K.

Physical insight was obtained into the results of Figures 2–7, after analysing the flame structure and conducting detailed reaction and species consumption path analyses.

In order to facilitate the discussion which is presented below, it should be noted that while reactions S1(OH), S2(O), and S3(H) have zero activation energies, reactions S4(CO_2) and S5(H_2O) have large activation energies, which are also nearly identical. Furthermore, the activation energy of S6(O_2) is large but lower than these of S4(CO_2) and S5(H_2O). Finally, reaction S5(H_2O) has a pre-exponential factor that is about 50 times larger compared to S4(CO_2). These comparisons of the kinetic parameters between the various heterogeneous reactions are based on the mechanism of Bradley *et al.* (1984).

For a given K, the increase of $R_{c,s}$ with T_s was found for all ϕs to be caused by the activation of reactions S4(CO_2), S5(H_2O), and S6(O_2), given that they are temperature-dependent and involve

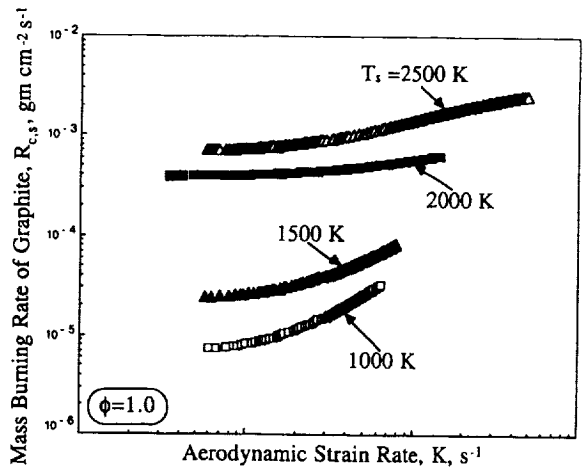

Figure 2. Effects of aerodynamic strain rate, K, and graphite surface temperature, T_s, on the mass burning rate of graphite, $R_{c,s}$, for a $\phi = 1.0$ flame.

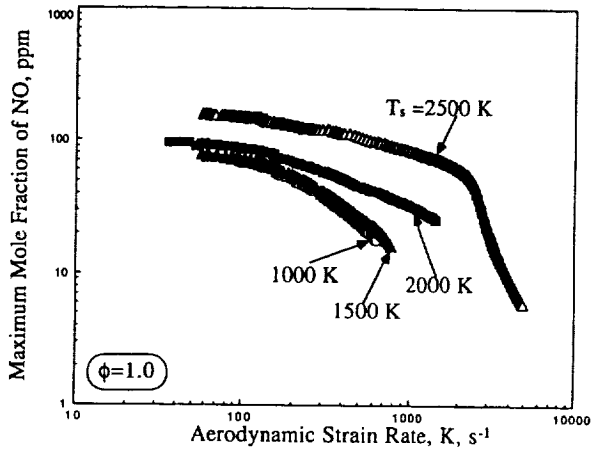

Figure 3. Effects of aerodynamic strain rate, K, and graphite surface temperature, T_s, on the maximum mole fraction of NO for a $\phi = 1.0$ flame.

stable species which can be present at high concentrations in the postflame region. Furthermore, for a given T_s, the increase of $R_{c,s}$ with K was found to be caused for all ϕs by the augmented reactant supply at the surface vicinity, given that large strain rates result to large species concentration gradients at the stagnation plane. At the same time, however, high strain rates can lead to incomplete reaction in the gas phase, and thus can affect the species concentrations at the stagnation plane, as it will be discussed later.

One of the main conclusions of this study is that the mechanisms responsible for the solid fuel consumption can substantially differ depending on the gas-phase composition, and that this

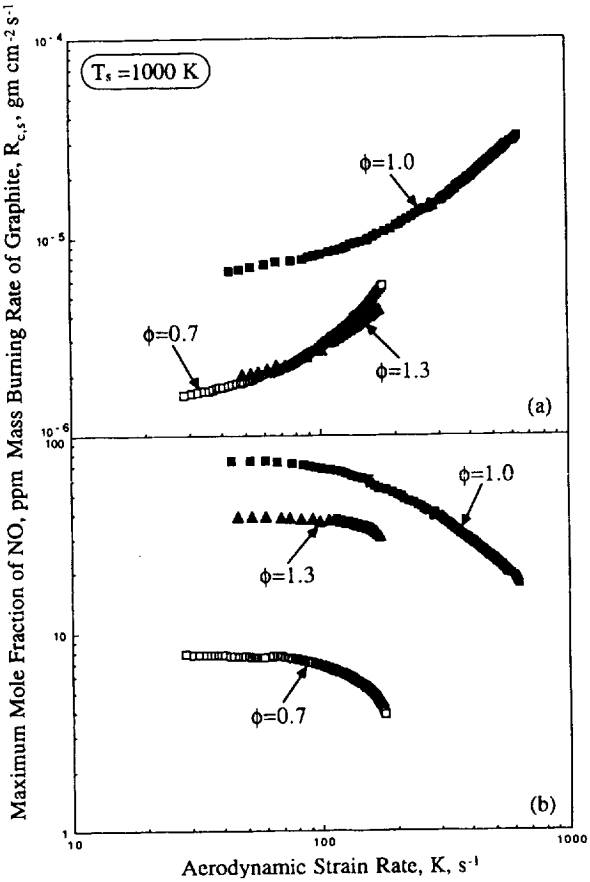

Figure 4. Effects of aerodynamic strain rate, K, and equivalence ratio, ϕ, on the mass burning rate of graphite, $R_{c,s}$, and the maximum mole fraction of NO for graphite surface temperature T_s = 1000 K.

dependence is further complicated by the magnitudes of both the strain rate and surface temperature. To this end, the fractional contribution of each gas-phase species to the consumption of the solid fuel was calculated as function of the strain rate at different surface temperatures. The results of these fractional contributions are shown in Figures 8, 9, and 10 for ϕ = 0.7, 1.0, and 1.3, respectively.

A general remark is that as K increases, the contributions of the stable species CO_2, H_2O, and O_2 to $R_{c,s}$ decrease in most cases. Physically, this happens because as K increases, the residence time is reduced, and the conversion of the intermediate species to stable equilibrium products such as CO_2 and H_2O is incomplete. Thus, as K increases the concentration of the stable equilibrium products is reduced at the surface, while the concentrations of the radicals increase.

The only exception to that is the initial (low Ks) increase of the fractional contribution of H_2O to $R_{c,s}$ at T_s = 2500 K for all ϕs. This fractional contribution subsequently levels off, and in some cases it slightly reduces as K increases.

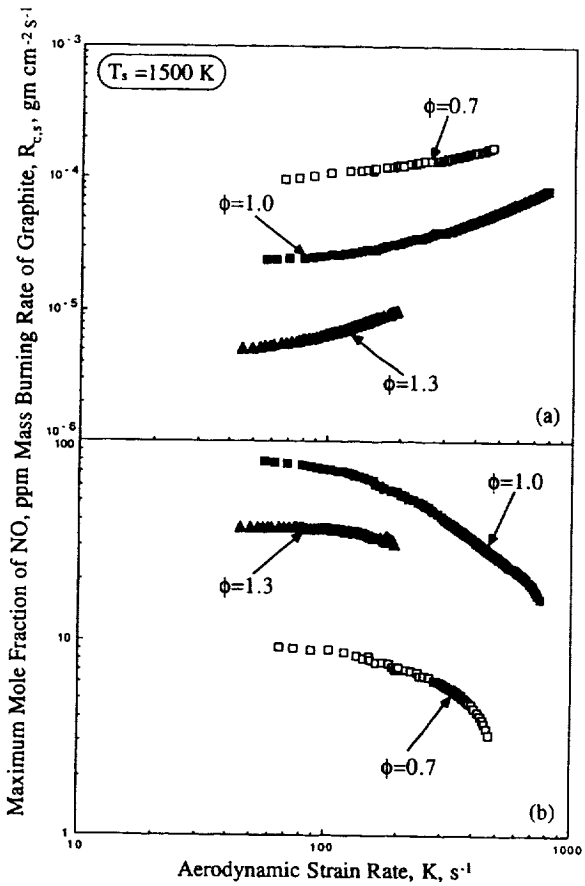

Figure 5. Effects of aerodynamic strain rate, K, and equivalence ratio, ϕ, on the mass burning rate of graphite, $R_{c,s}$, and the maximum mole fraction of NO for graphite surface temperature $T_s = 1500$ K.

The contribution of O_2 was found to decrease as K increases, because of the increased contributions of the OH, O, and H radicals. The only exception to that is the $\phi = 1.3$ flame at $T_s = 2000$ K, for which a rapid increase of the O_2 contribution is observed for $K > 500\ s^{-1}$. The large contributions of the OH, O, and H radicals to $R_{c,s}$ is caused by the large concentration of these radicals in the postflame region, especially at high strain rates. Such behaviour is not expected in a pure non-premixed oxidizing gas phase, as it was the case in the previous studies (Cho *et al.*, 1992; Lee *et al.*, 1995; Chelliah *et al.*, 1996).

It is also observed that in most cases the fractional contributions of the H, O, and OH radicals to $R_{c,s}$ decrease as K increases, because of the increase of the radical concentrations and their gradients at the surface, as mentioned earlier. The only exception is the response of the contribution of the OH radicals to strain rate for $\phi = 1.0$ at the lower $T_s = 1000$ and 1500 K. This was found to be a result of the steeper increase of the contribution of the H radicals with the strain rate for stoichiometric flames, in which the H radicals exist in larger concentrations compared to off-stoichiometric flames.

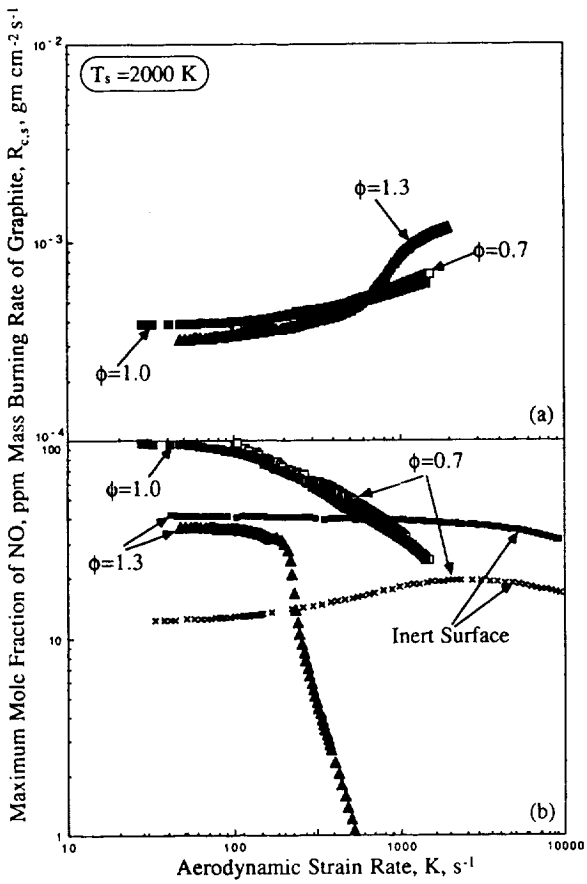

Figure 6. Effects of aerodynamic strain rate, K, and equivalence ratio, ϕ, on the mass burning rate of graphite, $R_{c,s}$, and the maximum mole fraction of NO for graphite surface temperature $T_s = 2000$ K.

For the fuel-lean, $\phi = 0.7$ flame it can be seen (Figure 8) that at $T_s = 1000$ K the $R_{c,s}$ results by 60 per cent from S1(OH) and by 20 per cent from S6(O_2) at low Ks, while at large Ks the S6(O_2) contributes only 10 per cent. For all Ks there is also a contribution of about 10 per cent from each S2(O) and S3(H), while S4(CO_2) and S5(H_2O) have no contributions. At $T_s = 1500$ K, S6(O_2) is activated and contributes 60 per cent at low Ks and 40 per cent at high Ks, while S1(OH), S2(O), and S3(H) contribute by amounts of 20, 5, and 10 per cent respectively. At $T_s = 1500$ K, the contribution of S5(H_2O) is 2 per cent, while S4(CO_2) has no contribution. At the higher temperatures of $T_s = 2000$ and 2500 K, S5(H_2O) contributes to $R_{c,s}$ by 80 per cent. At $T_s = 2000$ K, the balance of $R_{c,s}$ is due to S1(OH)(5–10 per cent), S3(H)(10–15 per cent), and S6(O_2)($\sim$ 3 per cent) while the contribution of S4(CO_2) becomes finite. At $T_s = 2500$ K, S4(CO_2) becomes more important contributing to the $R_{c,s}$ by 20 per cent at low Ks and 10 per cent at high Ks, while S3(H) has a contribution of about 10 per cent. At $T_s = 2500$ K, it can be seen that at low Ks the contribution of S5(H_2O) increases with K given that the graphite consumption is dominated by S4(CO_2) and S5(H_2O). The contribution of S4(CO_2) is reduced at high Ks because

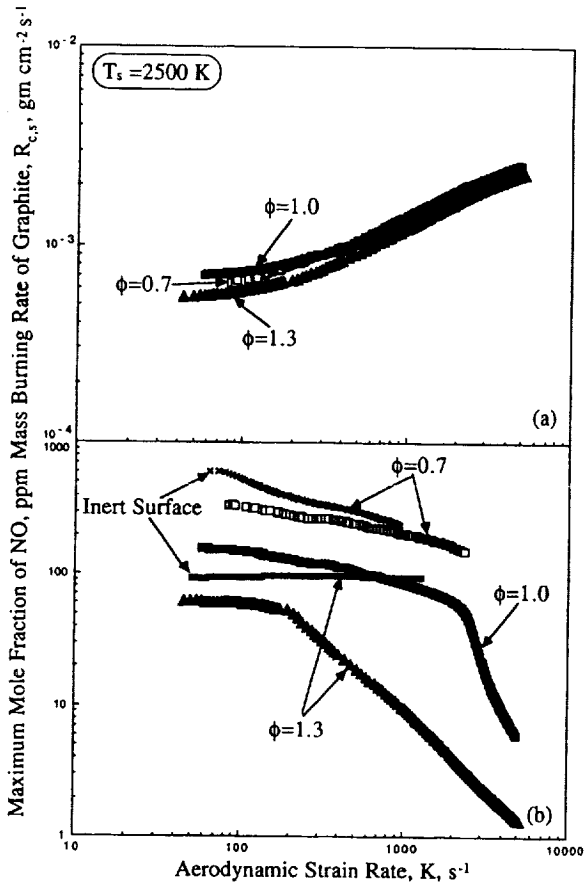

Figure 7. Effects of aerodynamic strain rate, K, and equivalence ratio, ϕ, on the mass burning rate of graphite, $R_{c,s}$, and the maximum mole fraction of NO for graphite surface temperature $T_s = 2500$ K.

of the reduced CO_2 production through the slow $CO + OH \rightarrow CO_2 + H$ gas-phase reaction. Subsequently, the S4(CO_2) contribution levels off and the increase of S5(H_2O) is arrested as K increases, and the extent of the conversion of H_2 to H_2O is reduced.

For the stoichiometric $\phi = 1.0$ flame it can be seen (Figure 9) that at $T_s = 1000$ and 1500 K, the $R_{c,s}$ is dominated by S3(H) because of the abundance of H radicals, and the fact that reactions S4(CO_2) and S5(H_2O) are not activated at these low graphite temperatures. At $T_s = 1000$ K, S1(OH) and S2(O) contribute by 20 and 7 per cent, respectively. At $T_s = 1500$ K, S1(OH) contributes 30 per cent, the contribution of S2(O) is reduced to 3 per cent, and the contribution of S5(H_2O) ranges from 8 per cent at low Ks to 4 per cent at high Ks. At $T_s = 1500$ K, S6(O_2) becomes important and contributes about 30 per cent at low Ks and about 20 per cent at high Ks. The contribution of S6(O_2) for the $\phi = 1.0$ flame at $T_s = 1500$ K is less compared to the $\phi = 0.7$ flame, given that for the $\phi = 1.0$ flame less O_2 survives the main reaction zone compared to the $\phi = 0.7$ flame. At $T_s = 2000$ and 2500 K, S5(H_2O) is dominant (80–90 per cent contribution), S3(H) contributes 10 per cent, while S4(CO_2) emerges as important at $T_s = 2500$ K.

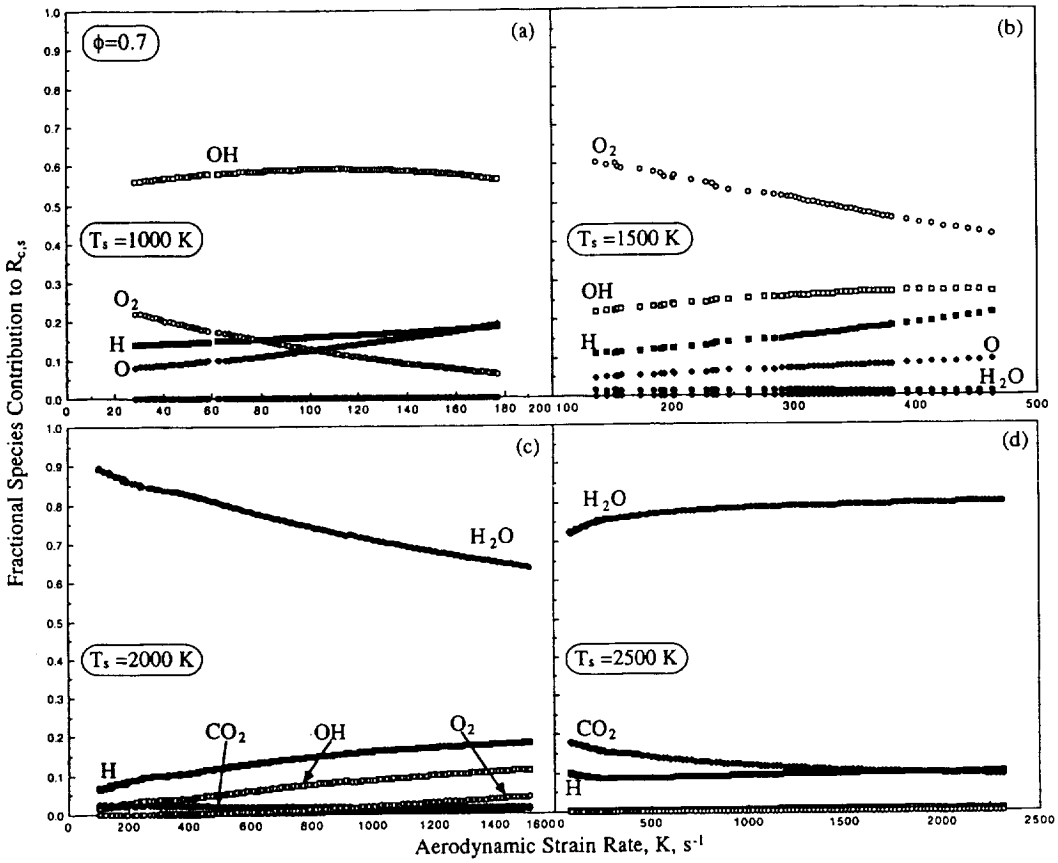

Figure 8. Effects of aerodynamic strain rate, K, and graphite surface temperature, T_s, on the fractional species contributions to the mass burning rate of graphite, $R_{c,s}$, for a $\phi = 0.7$ flame.

For the fuel-rich, $\phi = 1.3$ flame, it can be seen (Figure 10) that the contribution of S6(O_2) is minimum, which is reasonable given that there is lack of oxygen in the postflame region. Furthermore, because of the relative abundance of H radicals in fuel-rich flames (compared to O and OH) the contribution of S3(H) at $T_s = 1000$ K is nearly 100 per cent, and it is reduced to about 60 per cent at $T_s = 1500$ K at which S1(OH) and S5(H_2O) become important. At $T_s = 2000$ K and $K > 500\ s^{-1}$ the noticeable $R_{c,s}$ increase that was shown in Figure 6, was found to be a result of the extinction of the gas phase, which allows the O_2 to reach the graphite surface and readily contribute to the graphite consumption, resulting thus to a nearly 100 per cent consumption of the solid graphite by S6(O_2). At $T_s = 2500$ K, S5(H_2O) contributes 80 per cent, while S3(H) has a contribution of 10 per cent and S4(CO_2) contributes between 20 per cent at low Ks and 10 per cent at high Ks.

For both $\phi = 1.0$ and 1.3 flames the initial increase of the contribution of S5(H_2O) is similar to the one observed for the $\phi = 0.7$ flame, and the mechanism responsible for such behaviour is also the reduction of the S4(CO_2) contribution as K increases.

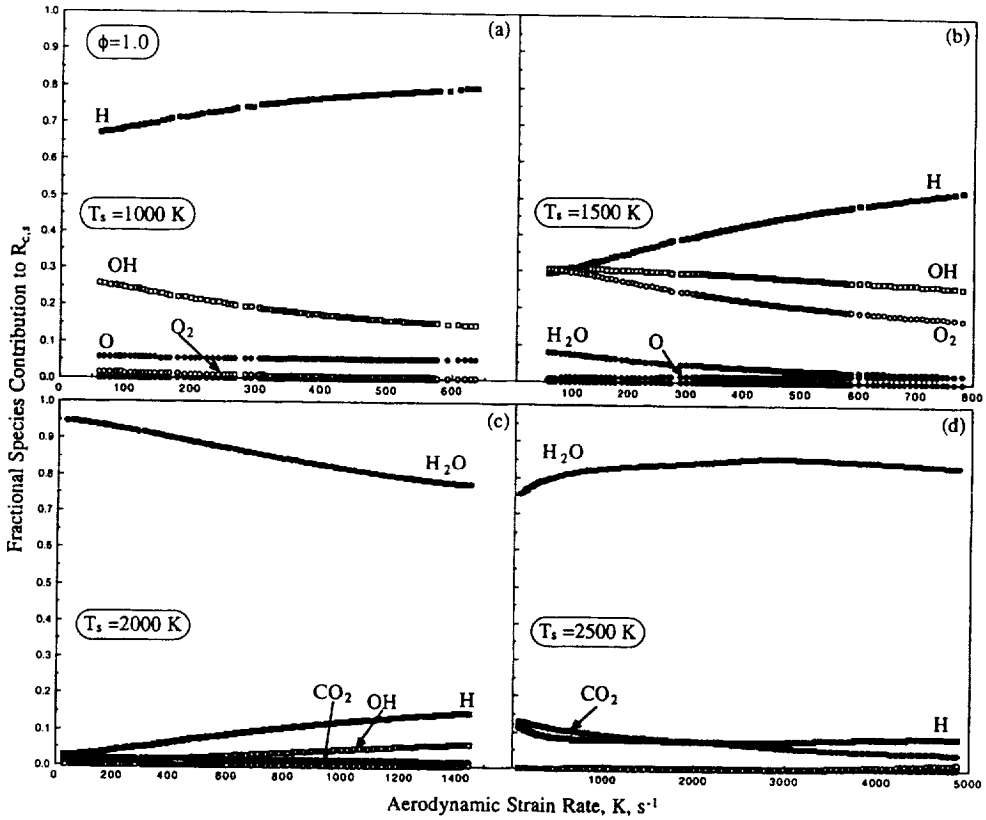

Figure 9. Effects of aerodynamic strain rate, K, and graphite surface temperature, T_s, on the fractional species contributions to the mass burning rate of graphite, $R_{c,s}$, for a $\phi = 1.0$ flame.

Based on these observations, a physical explanation can be now provided on the dependence of $R_{c,s}$ on ϕs for different T_ss as it is shown in Figures 4–7.

At $T_s = 1000$ K the $R_{c,s}$ for all ϕs is dominated by the reactions with OH($\phi = 0.7$) and H($\phi = 1.0$, 1.3) radicals, and the $\phi = 1.0$ flame results to a greater $R_{c,s}$ because of the larger radical concentrations. At $T_s = 1500$ K, however, the O_2-rich, $\phi = 0.7$ flame has a larger $R_{c,s}$ given that for this 'moderate' graphite surface temperature, S6(O_2) is activated and its rate becomes large.

At $T_s = 2000$ and 2500 K, S5(H_2O) dominates at all ϕs leading to $R_{c,s}$ of the same order. Physically, the contribution of reaction S5(H_2O) to $R_{c,s}$ dominates at these graphite temperatures the contribution of S4(CO_2) because (a) its specific reaction rate is about 50 times larger than this of S4(CO_2) and (b) for methane flames the H_2O molar concentration in the postflame zone is twice as much as this of CO_2. The contributions of S6(O_2) at these high graphite temperatures are reduced given that the O_2 is mainly consumed in the gas phase at the vicinity of the stagnation plane by the main branching reaction $H + O_2 \rightarrow OH + O$, which becomes particularly fast above 1800 K.

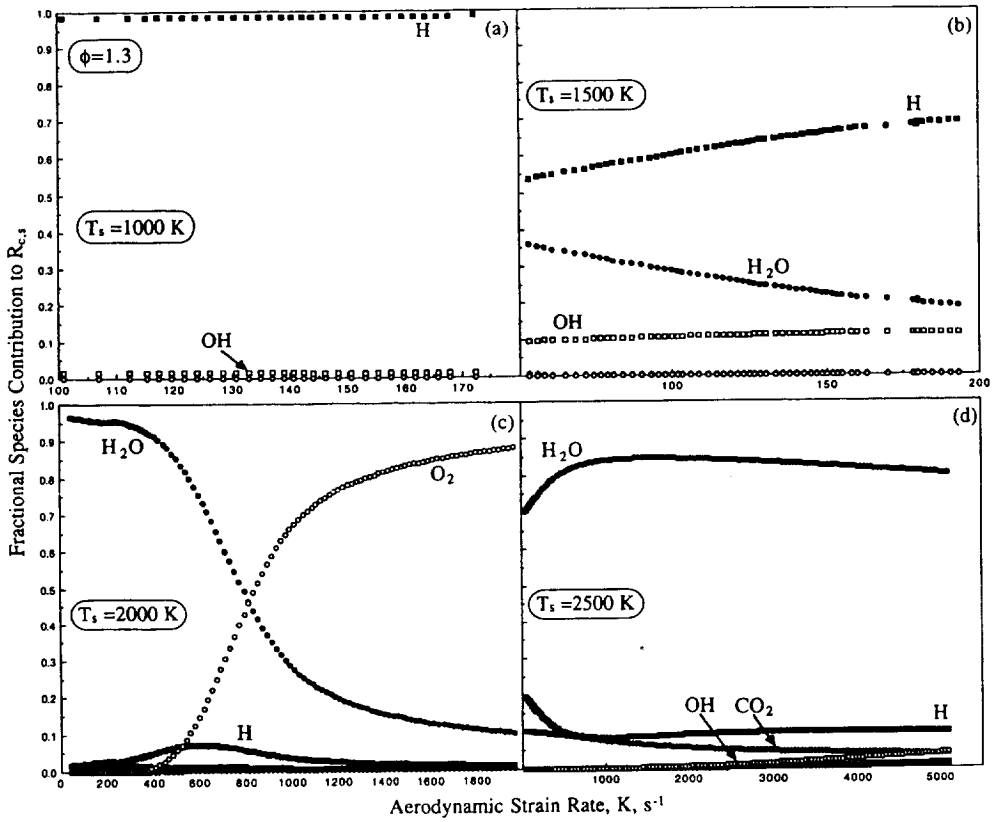

Figure 10. Effects of aerodynamic strain rate, K, and graphite surface temperature, T_s, on the fractional species contributions to the mass burning rate of graphite, $R_{c,s}$, for a $\phi = 1.3$ flame.

At all T_ss, the $\phi = 1.3$ flame has in general the lowest $R_{c,s}$ for two reasons. First, for fuel-rich flames the concentrations of O_2, H_2O, and CO_2 are low in the postflame region. Furthermore, the $\phi = 1.3$ methane/air flame has Le > 1 and it is extinguished while it is far from the surface, so that large species gradients do not develop next to the graphite surface. The exception to that is the case in which extinction of the gas phase occurs at high strain rates, and the $R_{c,s}$ increases substantially as it is shown in Figure 6 for $T_s = 2000$ K. Under such conditions, the O_2 will not be consumed in the main reaction zone, and it will be readily available for the graphite consumption so that S6(O_2) becomes dominant. The structure of $\phi = 1.3$ flame for $T_s = 2000$ K and at different strain rates can be seen in Figures 11 and 12. Figure 11 depicts that at the low $K = 201\ s^{-1}$ the O_2 is totally consumed in the flame zone, and that substantial amounts of H_2O form that subsequently are used for the graphite oxidation. As the strain rate increases, however, the gas-phase chemical activity is reduced, O_2 reaches the graphite surface and the H_2O concentration at the surface is reduced. Similarly, Figure 12 depicts that as the strain rate increases, there is a substantial reduction of the maximum H mass fraction because of the reduced chemical activity of the gas phase. The observed peak of the H mass fraction at the high strain rates is caused by the thermal decomposition of the CH_4 fuel at the surface vicinity.

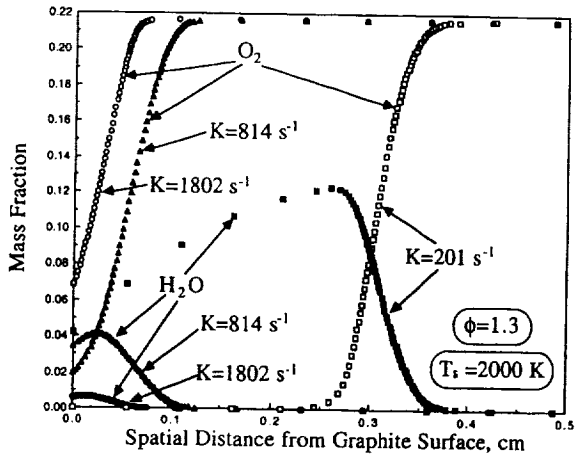

Figure 11. Effects of aerodynamic strain rate, K, on the O_2 and H_2O mass fraction profiles, for a $\phi = 1.3$ flame and $T_s = 2000$ K.

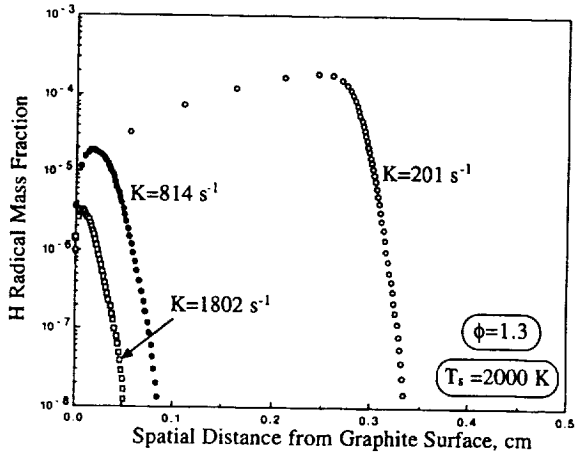

Figure 12. Effects of aerodynamic strain rate, K, on the H mass fraction profiles, for a $\phi = 1.3$ flame and $T_s = 2000$ K.

Effects on the nitrogen oxides

The $X_{NO,max}$ behavior observed in Figures 3–7 can be also explained. The increase of $X_{NO,max}$ with T_s is physically reasonable given that the NO formation kinetic steps have high activation energies and the gas-phase temperature increases with T_s as a result of the heat transfer between the two phases. Similarly, the observation that for $T_s = 1000$ and 1500 K $(X_{NO,max})_{\phi=0.7} < (X_{NO,max})_{\phi=1.3} < (X_{NO,max})_{\phi=1.0}$ is attributed to the flame temperature given that $T_{ad,\phi=0.7}(1838\,K) < T_{ad,\phi=1.3}(2086\,K) < T_{ad,\phi=1.0}(2225\,K)$. However, the $X_{NO,max}$ dependence on T_s was also found to be a function of ϕ, given that $X_{NO,max}$ was shown to substantially

increase from $T_s = 1500$ to 2000 K only for the $\phi = 0.7$ flame. Furthermore, for $T_s > 1500$ K $(X_{NO,max})_{\phi=1.3} < (X_{NO,max})_{\phi=1.0} < (X_{NO,max})_{\phi=0.7}$. Analysis of the detailed structure revealed that for all cases, the NO formation was a result of both the homogeneous and heterogeneous kinetic processes. These processes, however, were found to depend on both T_s and ϕ.

For the fuel-lean, $\phi = 0.7$ flame the initiation of NO formation was found to be due to the reactions

$$O + N_2 \rightarrow N + NO \quad (-R176)$$

$$CH + N_2 \rightarrow HCN + N, \quad (R238)$$

with the rate of $(-R176)$ being noticeably faster at temperatures above 1800 K. The variations of the rates of R176 and R238 and the mass fraction of NO, Y_{NO}, are shown for a $\phi = 0.7$ flame at a moderate $K = 250\ s^{-1}$ in Figures 13 and 14 for $T_s = 2000$ and 2500 K, respectively. First, it should be noted that the rate of (R176) increases significantly from $T_s = 2000$ to 2500 K as a result of the super-adiabaticity of the gas phase. It can be also seen that while in the main flame zone the relative importance between $(-R176)$ and (R238) is the anticipated one, next to the solid fuel there is a second peak of the rate of (R238). This second peak at the vicinity of the solid phase was found to be caused by the heterogeneous production of CH_4 via S3(H), which is active at all T_ss studied herein. The H radicals that are needed for the progress of S3(H) are provided by the gas phase chemical reactions, as well as by the heterogeneous processes. At $T_s = 1000$ and 1500 K, reaction S1(OH) contributes greatly to the C(s) consumption producing thus extra H radicals. At $T_s = 2000$ and 2500 K, C(s) is mainly consumed by S5(H_2O) releasing thus H_2 that results in H production through

$$O + H_2 \rightarrow H + OH \quad (R3)$$

$$OH + H_2 \rightarrow H + H_2O \quad (R83)$$

Subsequently, CH_4 reacts with O, H, and OH to produce CH_3, which is then converted to CH_2 through reactions with O and OH. CH_2 is then converted to CH, enhancing thus the rate of R238.

For the $\phi = 0.7$ flame at $T_s = 2000$ K, it was found that the NO forms through

$$O + N_2 \rightarrow N + NO \quad (10 \text{ per cent}) \quad (-R176)$$

$$N + OH \rightarrow NO + H \quad (60 \text{ per cent}) \quad (R178)$$

$$HNO + H \rightarrow NO + H_2 \quad (20 \text{ per cent}) \quad (R212)$$

The contributing percentages indicated within the parentheses were determined by spatially integrating all pertinent reaction rates. HNO was found to form through

$$NH + OH \rightarrow HNO + H \quad (26 \text{ per cent}) \quad (R190)$$

$$NH + H_2O \rightarrow HNO + H_2 \quad (65 \text{ per cent}) \quad (R195)$$

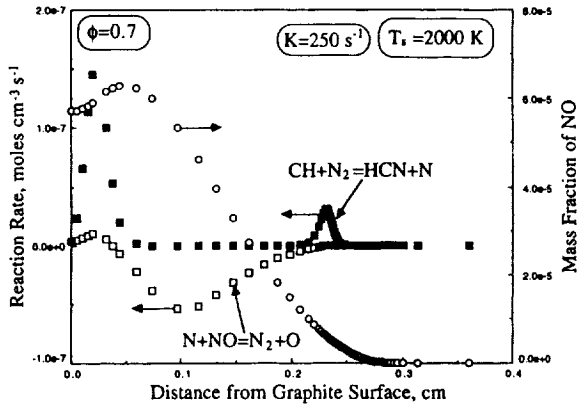

Figure 13. Spatial variations of the mass fraction of NO and the rates of $N + NO = N_2 + O$ and $CH + N_2 = HCN + N$ reactions, for a $\phi = 0.7$ flame at $K = 250\ s^{-1}$ and $T_s = 2000$ K.

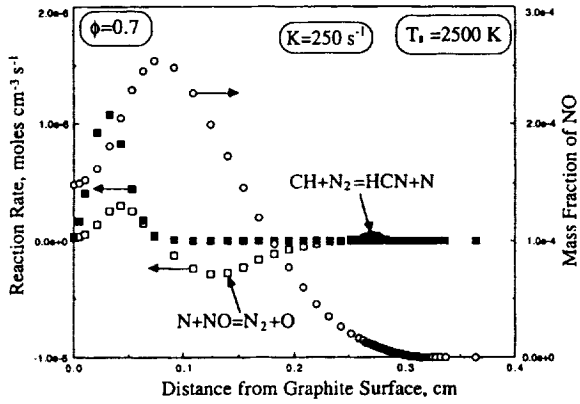

Figure 14. Spatial variations of the mass fraction of NO and the rates of $N + NO = N_2 + O$ and $CH + N_2 = HCN + N$ reactions, for a $\phi = 0.7$ flame at $K = 250\ s^{-1}$ and $T_s = 2500$ K.

while NH forms equally through

$$NH_2 + H \rightarrow NH + H_2 \quad (45 \text{ per cent}) \quad (R200)$$

$$NCO + H \rightarrow NH + CO \quad (45 \text{ per cent}) \quad (R221)$$

NH_2 forms almost entirely through

$$HNCO + H \rightarrow NH_2 + CO \quad (95 \text{ per cent}) \quad (R263)$$

while HNCO forms through

$$HOCN + H \rightarrow H + HNCO \quad (50 \text{ per cent}) \quad (R271)$$
$$CH_2 + NO \rightarrow H + HNCO \quad (30 \text{ per cent}) \quad (R247)$$

Finally, HOCN forms entirely through

$$HCN + OH \rightarrow HOCN + H \quad (100 \text{ per cent}) \quad (R232)$$

NCO was found to form through

$$CN + OH \rightarrow NCO + H \quad (40 \text{ per cent}) \quad (R216)$$
$$HCN + O \rightarrow NCO + O \quad (50 \text{ per cent}) \quad (R229)$$

with CN being produced directly from HCN.

These findings indicate the importance of (R238) to this kinetic sequence leading to NO. In both Figures 13 and 14, it can be also seen that Y_{NO} decreases at the vicinity of the solid phase for two reasons. First, there is local dilution effect next to the surface, which is caused by the intense gasification of the solid phase at these high T_ss. Second, chemical reactions which reduce NO are activated, as it will be shown below.

Analysis of the fuel-rich, $\phi = 1.3$ flame shows that the initiation of NO formation is entirely due to (R238) at all T_ss, and the double pick of (R238) is also observed especially at $T_s = 2500$ K. At $T_s = 1000$ and 1500 K, the graphite is mainly consumed by S3(H), with the H radicals being supplied by the flame since no heterogeneous H-producing mechanism is active. At $T_s = 2000$ K, S5(H_2O) is activated and the produced H_2 is converted to H through (R83). However, the rate of (R83) is low because of the reduced OH concentrations. At $T_s = 2500$ K, S5(H_2O) is enhanced resulting in greater production of H_2, so that (R83) is enhanced. Thus, H radicals are produced, S3(H) becomes important and CH_4 is produced. Furthermore, at $T_s = 2500$ K, CH_4 readily decomposes to CH_3 and H increasing, thus, the local CH_3 and H radical pools. Subsequently, H results to more CH_4 production through S3(H), while CH_3 is converted to CH_2 and finally to CH either through recombination to C_2 species or though reaction with H. Thus, the concentration of CH and, as a result, the rate of (R238) are enhanced.

For the $\phi = 1.3$ flame, the NO formation was found to be caused by HNO reactions, namely its thermal decomposition (R210) by an amount of 50 per cent and (R212) by an amount 27 per cent. The contribution of (R178) to NO is only 22 per cent because of the reduced OH concentration. HNO was found to be produced almost entirely by (R195) with the sequence proceeding the formation of NH (needed by (R195)) being similar to the one already described.

The comparisons depicted in Figures 6 and 7 for the $X_{NO,max}$ between the graphite and the inert surface indicate that the simultaneous burning of graphite and methane can potentially lead to NO_x reduction. It was found that this is caused by the heterogeneous production of CH_4, which subsequently results to increased concentrations of CH_3, CH_2, CH, and N radicals at the vicinity of the surface, and which locally enhance NO-reducing reactions. Obviously, such reactions are not present when the surface is a chemically inert one.

For the O_2-rich $\phi = 0.7$ flame, it was found that for $T_s \leqslant 2000$ K the O concentration next to the graphite surface is greater compared to the inert surface. This is caused by the additional

production of H radicals from the surface reactions, which in turn enhance locally the rate of the main branching reaction $H + O_2 \rightarrow OH + O$, which is primarily responsible for the production of O radicals. Thus the rate of $-$ R176 and R178 are enhanced compared to the inert surface and $X_{NO,max}$ increases. At $T_s > 2000$ K, the surface production of CH_4 increases and the resulting CH_2, CH, and N radicals reduce NO through reactions (R176) and (247) and

$$CH + NO \rightarrow HCN + O \quad \text{(R244)}$$

The reduction through R176 can be seen in Figures 13 and 14 at the surface vicinity where the rate of (R176) assumes positive values. Furthermore, for the inert surface and for $T_s > 2000$ K, the rate of ($-$ R176) increases substantially with T_s resulting thus in higher $X_{NO,max}$ compared to the graphite surface.

For the fuel-rich, $\phi = 1.3$ flame, it was found that the reduced O concentrations result in a slow rate for reaction ($-$ R176). Furthermore, it was found that for all T_s's the $X_{NO,max}$ values are lower for the graphite surface compared to the inert one because of the heterogeneous CH_4 production, which results in increased concentrations of CH_3 and CH_2. For this case, the reduction of NO takes place through

$$CH_3 + NO \rightarrow HCN + H_2O \quad \text{(R253)}$$

and R247 (CH_2 + NO), respectively.

The aforementioned results on the effect of heterogeneous processes on the NO, must be viewed with the understanding that in realistic carbon burning conditions (e.g. cofiring), additional mechanisms will be important. Such mechanisms include the NO_x production by fuel-bound nitrogen and NO_x reduction through adsorption and catalytic reaction with active sites on the graphite surface. The present results, however, may be viewed as one possible contribution to the entire NO_x reduction process. Ideally, future studies should address the details of these additional mechanisms.

Finally, the effect of strain rate on the concentration of NO was also analyzed. It was found that as K increases, the flame approaches the stagnation plane. Thus, for high Ks the residence time is reduced, and that results in reduced temperatures and $X_{NO,max}$ compared to the low Ks, given that the slow CO oxidation and NO-producing reactions cannot be completed. Furthermore, when T_s is lower than the flame temperature, there is conductive heat loss from the gas phase, which is enhanced at large Ks. Thus, at high Ks the gas-phase temperatures and $X_{NO,max}$ values will be lower. The abrupt reduction of $X_{NO,max}$ for $K > 200\,s^{-1}$ for the $\phi = 1.3$ flame (Figures 6 and 7) and for $K > 2500\,s^{-1}$ for the $\phi = 1.0$ flame (Figure 7), was found to be caused by the initiation of the gas-phase extinction process, which results to reduced gas phase-temperatures.

4. CONCLUSIONS

In this study, a numerical simulation was conducted on the steady burning of a solid fuel in premixed atmospheres, in the presence of strain rate. The investigation included the model case of solid graphite burning in a steady, stagnation flow of methane/air mixtures given that reasonable multi-step, semi-global heterogeneous kinetics are available for graphite, while the detailed

kinetics of methane are considered to be well-established. The parameters of interest were the graphite temperature, the gas-phase equivalence ratio, and the aerodynamic strain rate. The effects of these parameters on the graphite burning rate and the NO_x production and destruction mechanisms were assessed.

The results showed that the solid-phase temperature, the gas phase equivalence ratio, and the imposed strain rate, have a significant effect on both the graphite burning rate and the NO_x production. More specifically, it was found that as the solid phase temperature increases both the burning rate and NO concentration increase. Furthermore, as the strain rate increases, the graphite burning rate increases, while the NO_x concentration decreases. The effect of equivalence ratio was found to be non-monotonic, given that it affects the chemical composition at the solid-phase vicinity, modifying thus the controlling mechanisms of both the graphite burning rate and NO_x production and destruction. One of the most profound effects of the gas phase conditions on the graphite burning was found to occur when extinction of the gas phase is initiated, as it can affect dramatically the chemical composition at the vicinity of the solid surface.

The analysis of the detailed structure of the chemically active zones showed that the NO concentration is controlled by N radical-producing reactions both in the main flamc zone as well as at the solid surface. This behaviour was also found to be a function of the equivalence ratio and the solid-phase temperature. Finally, the surface chemical activity was found to result in most cases in reduced NO_x concentrations compared to inert surfaces.

The results of this study should be viewed with the understanding that the semi-global kinetics of graphite used herein are not yet well-established. Furthermore, in practical cases, such as carbon burning, there will be other important mechanisms such as fuel-bound nitrogen and solid-phase porosity. However, the goal of this study was to demonstrate the importance of the gas-phase conditions on the solid-fuel burning in premixed atmospheres. This system is far more complex compared to solid-fuel burning in pure oxidizing atmospheres. An additional parameter that will be addressed in a future investigation, is the effect of the far-field velocity, concentration, and temperature unsteadiness on the solid-fuel burning response. Far-field unsteadiness introduces additional time scales, which can couple with the ones of relevance to the kinetics and the molecular transport at the surface as well as in its vicinity.

ACKNOWLEDGEMENTS

This work was supported by NASA under Grant NAG3-1877 and the Fred W. O'Green Assistant Professorship in Engineering.

REFERENCES

Bowman CT, Frenklack M, Gardiner W, Smith G. 1995. The GRI 2.1 mechanism. Personal communications.

Bradley D, Dixon-Lewis G, El-Din Habik S, Mushi EMJ. 1984. The oxidation of graphite powder in flame reaction zones. *Twentieth Symposium (International) on Combustion*, The Combustion Institute, 931–940.

Chelliah HK, Makino A, Kato I, Araki N, Law CK. 1996. Modeling of graphite oxidation in a stagnation-point flow field using detailed homogeneous and semiglobal heterogeneous mechanisms with comparisons to experiments. *Combustion and Flame*, **104**:469–480.

Cho SY, Yetter RA, Dryer FL. 1992. A computer model for one-dimensional mass and energy transport in and around chemically reacting particles, including complex gas-phase chemistry, multicomponent molecular diffusion, surface evaporation, and heterogeneous reaction. *Journal of Computational Physics* **102**:160–179.

Egolfopoulos FN. 1994a. Dynamics and structure of unsteady, strained, laminar, premixed flames. *Twenty-Fifth Symposium (International) on Combustion*, The Combustion Institute, 1365–1373.

Egolfopoulos FN. 1994b. Geometric and radiation effects on steady and unsteady strained laminar flames. *Twenty-Fifth Symposium (International) on Combustion*, The Combustion Institute, 1375–1381.
Egolfopoulos FN, Zhang H, Zhang Z. 1997. Wall effects on the propagation and extinction of strained, laminar, premixed flames. *Combustion and Flame* **109**:237–252.
Egolfopoulos FN, Campbell CS. 1999. Dynamics and structure of dusty reacting flows: inert particles in strained, laminar, premixed flames. *Combustion and Flame* **117**:206–226.
Honda L, Ronney PD. 1996. Effect of ambient atmosphere on flame spread in microgravity. Western States Section/ Combustion Institute, University of Southern California, Los Angeles, CA, 28–29 October.
Kee RJ. 1992. Personal communications.
Kee RJ, Rupley FM, Miller JA. 1989. Chemkin-II: a fortran chemical kinetics package for the analysis of gas-phase chemical kinetics. *Sandia Report SAND*89-8009.
Kee RJ, Warnaz J, Miller JA. 1983. A FORTRAN computer code package for the evaluation of gas-phase viscosities, conductivities, and diffusion coefficients. *Sandia Report SAND*83-8209.
Law CK. 1988. Dynamics of stretched flames. *Twenty-Second Symposium (International) on Combustion*, The Combustion Institute, 1381–1402.
Lee JC, Yetter RA, Dryer FL. 1995. Transient numerical modeling of carbon particle ignition and oxidation. *Combustion and Flame* **101**:387–398.
Makino A, Law CK. 1986. Quasi-steady and transient combustion of a carbon particle: theory and experimental comparisons. *Twenty-First Symposium (International) on Combustion*, The Combustion Institute, 183–191.
Ronney PD, Greenberg JB, Zhang Y, Roegner EV. 1994. Flame spread over thin solid fuels in partially premixed atmospheres. *Twenty-Fifth Symposium (International) on Combustion*, The Combustion Institute, 474–484.
Walker Jr PL, Rushinko Jr F, Austin LG. 1959. *Advances in Catalysis and Related Subjects*, vol. XI. Academic Press: New York.